Available online at www.sciencedirect.com

SCIENCE DIRECT®

International Journal of Fatigue 28 (2006) 1413–1419

International Journal of Fatigue

www.elsevier.com/locate/ijfatigue

Fatigue behavior of Al_2O_3-based composite with $BaTiO_3$ piezoelectric phase

Sirirat Rattanachan [a,*], Yukio Miyashita [b], Yoshiharu Mutoh [b]

[a] Institute of Engineering, Suranaree University of Technology, 111 University Avenue, Muang, Nakron Ratchasima 30000, Thailand
[b] Department of Mechanical Engineering, Nagaoka University of Technology, 1603-1 Kamitomioka, Nagaoka-shi 940-2188, Japan

Available online 20 March 2006

Abstract

Fatigue behavior of Al_2O_3-based composite with $BaTiO_3$ piezoelectric phase was studied by carrying out four-point bending fatigue tests for the poled and unpoled composites, which was compared to that of monolithic Al_2O_3. Tests were conducted under load ratio of $R = 0.1$ at frequency of 20 Hz with sinusoidal waveform. The present composites exhibited high fatigue resistance compared to monolithic Al_2O_3. From the detailed observations, it was found that the improvement of fatigue strength was mainly due to stress-induced domain switching. The relationship between da/dN and K_{max} was evaluated by conducting fatigue crack growth tests. The threshold stress intensity factors for unpoled and poled composites were higher than that of monolithic Al_2O_3.
© 2006 Elsevier Ltd. All rights reserved.

Keywords: Fatigue; Crack growth behavior; Piezoelectric composite; Barium titanate; Alumina

1. Introduction

In recent years, new functional composites, such as composites with piezoelectric secondary phases, have been increasingly interested. Ceramic composites with functional materials as dispersoids have been found to improve the mechanical properties, and also some new functions can be introduced into the structural ceramic materials [1–3]. For ferroelectric/piezoelectric ceramics, domain switching can be caused by mechanical stress and/or electric field. The domain switching plays an important role on the toughening mechanism in $BaTiO_3$ and PZT ferroelectric ceramics [4,5]. However, there have been few studies on toughening mechanisms in the composites. In the previous work [6], $BaTiO_3$–Al_2O_3 composites could be produced by using a spark plasma sintering method. The dense composites could be obtained compared to those by the conventional pressure-less sintering method. The fracture toughness of the $BaTiO_3$–Al_2O_3 composites was improved and the highest fracture toughness of 6.04 MPa $m^{1/2}$ for the Al_2O_3 composite with 5 mol% $BaTiO_3$ was achieved, while that of the monolithic Al_2O_3 was 4 MPa $m^{1/2}$.

An electric field can switch a domain by either 180 or 90°, while a stress can switch a domain by only 90°. A 180° domain switching can cause a direct change of polarization and leads to a change of piezoelectric compliance tensor. A 90° domain switching can cause a direct change of both polarization and strain. Domain switching is associated with the domain wall movement. Experiments showed that when an electric potential or a mechanical load exceeded a critical value, the domain wall began to move and the amount of movement was related to the intensity of the load [8]. Effects of stress on the piezoelectric capabilities of lanthanum-doped lead zirconium titanate (PLZT) ceramics have demonstrated that the applied external compressive stress can lead to the disappearance of the hysteresis loop behavior by complete inhibition of 90° domain movement [8]. Therefore, the high level mechanical stressing of PZT produces irreversible deformation by the irreversible switching of 90° domains. This leads anisotropic deformation behavior in poled materials. The cyclic stressing of PZT may cause significant incremental increase in the irreversible strain. This behavior may also result in

* Corresponding author. Tel.: +66 44 224489; fax: +66 44 224220.
E-mail address: sirirat.b@sut.ac.th (S. Rattanachan).

0142-1123/$ - see front matter © 2006 Elsevier Ltd. All rights reserved.
doi:10.1016/j.ijfatigue.2006.02.022

electromechanical fatigue effect that causes the degradation of piezoelectric property.

As mentioned above, there have been some works on fatigue behavior of monolithic piezoelectric. However, no work on fatigue behavior of piezoelectric composites has been reported. Therefore, basic fatigue behavior and effect of piezoelectric property on fatigue strength and fatigue mechanisms have not been cleared. In the present study, four-point bending fatigue tests were conducted to investigate the fatigue behavior of $BaTiO_3$–Al_2O_3 composites as well as those of monolithic Al_2O_3 and $BaTiO_3$ ceramics. Fatigue tests were conducted on both the poled and unpoled samples. The fatigue crack growth behavior was also investigated and the piezoelectric effect on fatigue growth behavior was discussed.

2. Experimental procedure

2.1. Material preparation and microstructure

The Al_2O_3-based composite with 5 mol% $BaTiO_3$, which is termed as 95A5B composite, was fabricated. To mix two kinds of powders, ethanol was used and blended completely by ball mill for 24 h. The mixture was placed in a rotary vacuum evaporator to extract the solvent. A dry powder mixture sieved through 150 μm mesh screen was produced. The mixed powders were put into a cylindrical graphite die with an inner diameter of 25 mm, which was on the vibration table for homogeneous packing of the powders, with graphite punches on both sides and then sintered by using a spark plasma sintering machine under an applied load of 38 MPa in vacuum. The temperature was increased at a rate of 100 °C/min up to a sintering temperature of 1300 °C. After holding for 5 min at the sintering temperature, the d.c. power was shut off to let the sintered material rapidly cool to 600 °C for 30 min. The monolithic Al_2O_3 and $BaTiO_3$ were sintered by the same sintering process as the composite at 1300 and 1100 °C, respectively, under an applied load of 38 MPa.

Microstructures of the three materials sintered in the present study are shown in Fig. 1. Average grain sizes of monolithic Al_2O_3 and $BaTiO_3$ were 1–4 and 1–2 μm, respectively, as seen in Fig. 1(a) and (b). From the XRD analysis, the intermediate phases, $BaAl_6TiO_{12}$ and $BaAl_{13.2}O_{20.8}$, were found in this composite [6]. The different phases indicated the different colors, as can be seen in Fig. 1(c): dark, gray, and bright regions are Al_2O_3, intermediate and $BaTiO_3$ phases, respectively. Mechanical properties of the sintered materials are summarized in Table 1.

2.2. Specimen preparation

The sintered materials were cut into test specimens with dimensions of 3 × 4 × 35 mm. Both poled and unpoled 95A5B composites were prepared. Silver paste was applied on the 3 × 35 mm surface as electrode and dried in air oven at 120 °C for 10 min. The specimens were poled (1.25 kV/mm) parallel to the width of the specimen, as schematically shown in Fig. 2. For poling of the composite, the applied electric potential was significantly higher than that of monolithic $BaTiO_3$ (0.5–0.6 kV/mm) due to much smaller relative permittivity of Al_2O_3 phase. These values of electric potential for poling correspond to the maximum point, over which the electric current suddenly increases. Then, a surface crack in the width direction was introduced at the center of the tension side of the

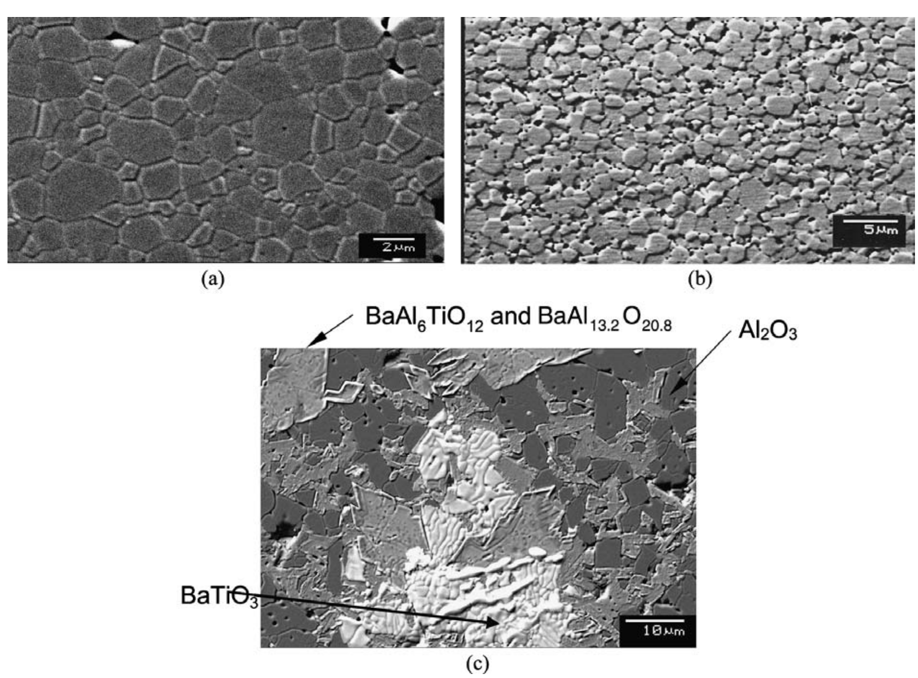

Fig. 1. Microstructures of the materials used in this study: (a) Al_2O_3, (b) $BaTiO_3$, and (c) 95A5B.

Table 1
Mechanical properties of the materials used in this study

	Al_2O_3	$BaTiO_3$	95A5B composite
Bending strength (MPa)	446.5	116.5	237.2
Fracture toughness (MPa m$^{1/2}$)	3.55–4.0	0.6–1.06	5.21–6.04
Young's modulus (GPa)	353	62.6	239
Poisson's ratio	0.175	0.41	0.23
Vickers hardness (GPa)	16.7	4.9	12.1

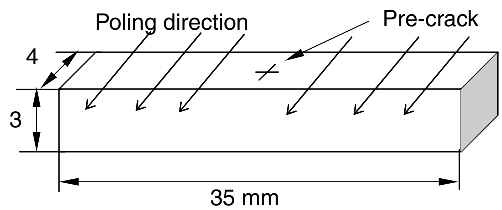

Fig. 2. Schematic of the dimensions of specimen and the direction of poling.

test specimen with a Vickers indenter using loads of 196 N for Al_2O_3 and 95A5B composite, and 4.9 N for $BaTiO_3$. The residual stress was removed by polishing more than three times of the depth of the Vickers impression from the surface [7]. Fig. 3 shows a micrograph of surface pre-crack for the poled 95A5B composite after removing the surface layer. The pre-crack lengths parallel to the poling direction were approximately 400 μm for 95A5B composite and monolithic alumina, and 120 μm for monolithic $BaTiO_3$. After polishing, the residual stress was measured by using an X-ray stress analysis method. Al_2O_3 phases located around a crack were measured as a diffraction phase. The diffraction from Al_2O_3 (146) plane by Cu-Kα was recorded with the side-inclination method. The X-ray stress constant (s) was calculated from various applied stresses (σ_A) of the alumina sample to determine stress by the $\sin^2\psi$ method

$$s = -\frac{E}{2(1+\upsilon)} \cot \theta_0,$$

where E and υ is elastic modulus and Poisson's ratio of alumina, respectively. θ_0 is the diffraction angle for stress-free materials. The stress was evaluated from the slope M of the $\sin^2\phi$ diagram as

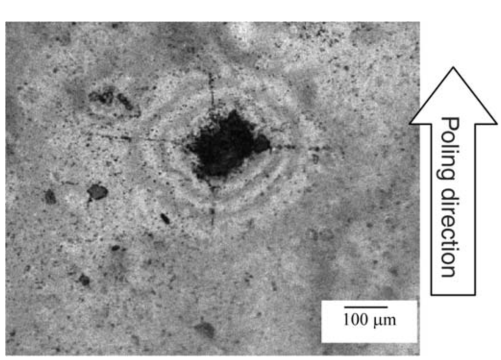

Fig. 3. Pre-crack observation by the replica method for the poled 95A5B composite.

$$\sigma_x = S \cdot M.$$

The residual stresses determined are summarized in Table 2. From Table 2, the presence of residual stress is found after Vickers indentation. However, after polishing, the residual stress was reduced to the same level as that before indentation. Therefore, it was suggested that the residual stress near the pre-crack was removed after polishing.

2.3. Fatigue test

The specimens were subjected to the four-point bending cyclic load on a servohydraulic fatigue machine with the loading conditions: sinusoidal waveform, load ratio (R) of 0.1 and frequency of 20 Hz. Fatigue tests were periodically interrupted to examine the crack growth behavior until failure. Crack lengths were measured by a replica method and the crack path was observed by using laser and optical microscopes. Data were presented in terms of the crack growth rate per cycle, da/dN, as a function of the maximum stress intensity factor, K_{max}, which was evaluated by the equation for a surface crack given by Newman and Raj [9].

3. Results and discussion

3.1. S–N curve

The relationships between maximum stress and number of cycles to failure for Al_2O_3, poled and unpoled 95A5B as well as poled and unpoled $BaTiO_3$ samples are shown in Fig. 4. The specimens which did not fail up to 10^6 cycles are marked by the arrow symbol (→). As can be seen from Fig. 4, the fatigue limits of unpoled and poled 95A5B were noticeably higher than that of monolithic Al_2O_3. The fatigue limits at 10^6 cycles were 77 MPa for monolithic Al_2O_3 and 90 MPa for unpoled and poled 95A5B. At higher stress level, the fatigue strengths of these three specimens almost coincided. For monolithic $BaTiO_3$, the fatigue limits at 10^6 cycles were 30 MPa for unpoled one and 46 MPa for poled one.

3.2. Fatigue crack growth curve

Fig. 5 indicates the relationships between crack growth rate (parallel to the poling direction), da/dN, and maximum stress intensity factor, K_{max}, for unpoled and poled $BaTiO_3$. The initial and final aspect ratios on the fracture

Table 2
Residual stress for the Al_2O_3 specimens by the X-ray stress measurement method

	Residual stress (MPa)
On surface without crack	46.7
Near crack before polishing	93.9
Near crack after polishing	34.3

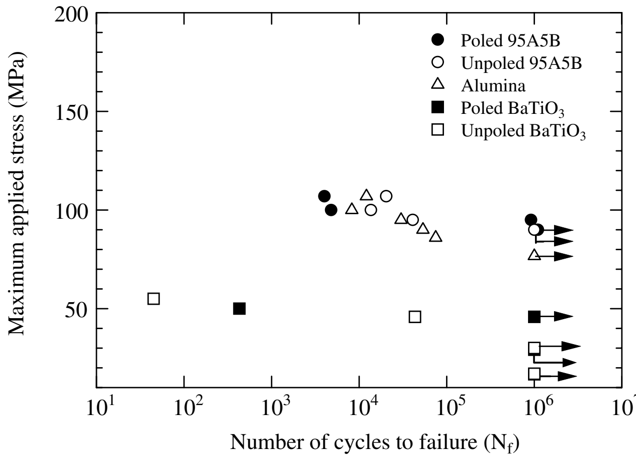

Fig. 4. S–N curves for monolithic Al_2O_3, $BaTiO_3$, and 95A5B composites.

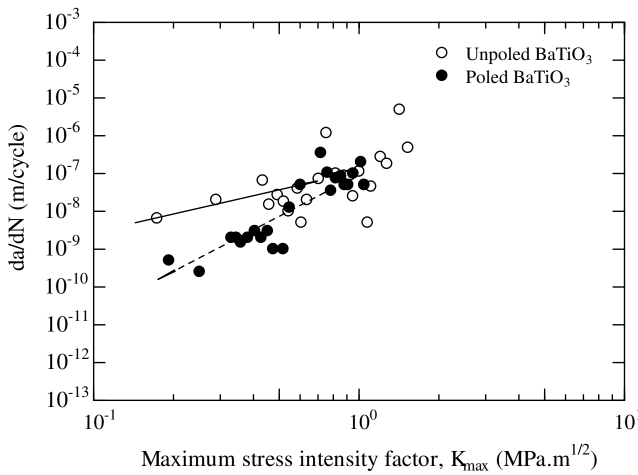

Fig. 5. Relationship between da/dN and maximum stress intensity factor for unpoled and poled $BaTiO_3$.

surface were measured and it was found that both of ratios were almost the same. In this paper, the aspect ratio was assumed to be 0.7 and almost constant during crack growth. As can be seen from the figure, the crack growth rate for poled $BaTiO_3$ was lower than that for unpoled one in the low K_{max} region. In the high K_{max} region, no significant difference of crack growth rate was found between unpoled and poled $BaTiO_3$. This crack growth behavior indicates that the toughening due to the stress-induced domain switching exhibits at the low stress intensity factors, while this toughening mechanism is degraded at the high stress intensity factors due to the accumulation of the irreversible deformation of 90° domain switching. This crack growth behavior is consistent with the S–N curves for poled and unpoled $BaTiO_3$ shown in Fig. 4, where the fatigue limit of poled $BaTiO_3$ is higher than that of unpoled one but the fatigue strengths of both the specimens almost coincide at high stress level.

The relationships between da/dN and K_{max} for monolithic Al_2O_3, unpoled and poled 95A5B are shown in Fig. 6. Arrows in this figure indicate the threshold values,

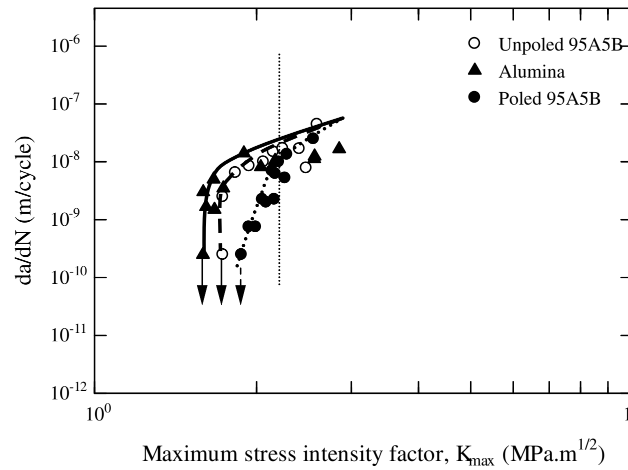

Fig. 6. Relationship between da/dN and maximum stress intensity factor for monolithic Al_2O_3, unpoled, and poled 95A5B composites.

K_{th}, of each sample. As can be seen from the figure, the crack growth rate of poled 95A5B was significantly low compared to those of unpoled 95A5B and monolithic Al_2O_3 in the low K_{max} region, while they almost coincided each other in the high stress intensity factor region. This result was similar to that for the monolithic $BaTiO_3$. This crack growth behavior was almost consistent with the fatigue behavior observed in S–N curve, while the difference of fatigue limit between poled and unpoled 95A5B was not significant.

3.3. Fracture surface

Scanning electron microscopy observations of fatigue surfaces for the monolithic Al_2O_3 (Fig. 7(a)) revealed predominant intergranular fracture while intergranular with some transgranular regions was dominant in the unstable fracture region (Fig. 7(b)). Fig. 8 shows scanning electron micrographs for fatigue surface of unpoled 95A5B. Corresponding to the composition of 95A5B composite, liquid phases appear at grain boundaries during sintering process, which enhance the grain growth [6]. Fatigue fracture surface showed intergranular fracture at Al_2O_3 grains mixed with transgranular fracture at reaction phases. It can be found no significant difference of fracture surface morphology between the fatigue crack growth region and the final unstable fracture region.

3.4. Crack path

From the scanning electron microscopy observations, an example of fatigue crack path for unpoled 95A5B is shown in Fig. 9. From the figure, dominant intergranular crack path was found with existence of grain bridging on the crack wake. In addition, the crack in the threshold region was arrested at or near the reaction phase as same as the case for fracture toughness tests [6]. The similar fatigue crack path was also observed in the poled sample.

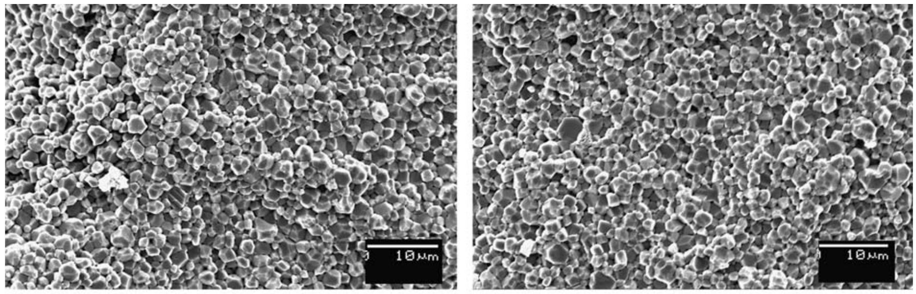

(a) (b)

Fig. 7. SEM micrographs of fracture surface for Al_2O_3: (a) fatigue crack growth region and (b) unstable fracture region.

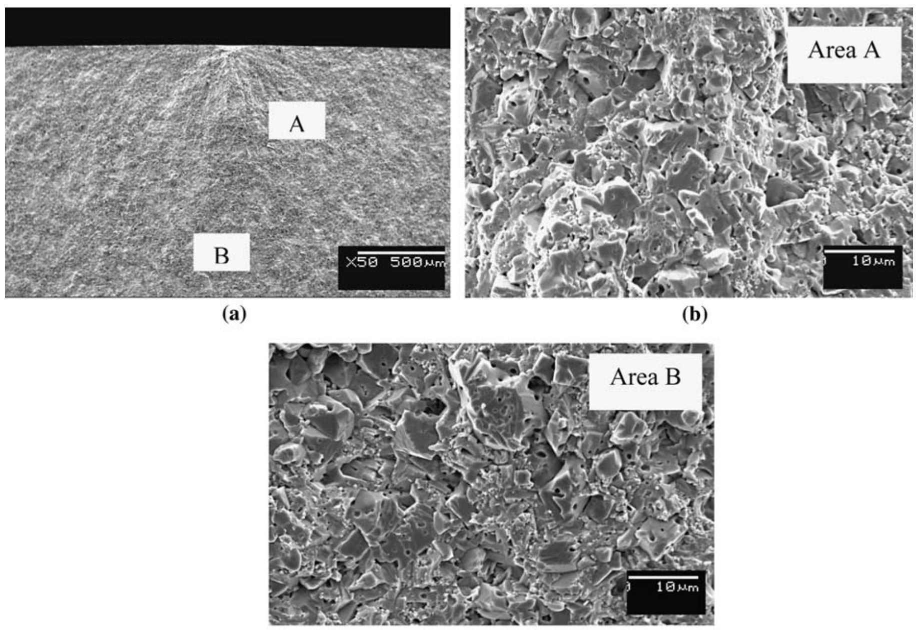

(a) (b) (c)

Fig. 8. SEM micrographs of fracture surface for unpoled 95A5B composite: (a) overview, (b) area A: fatigue crack growth region, and (c) area B: unstable fracture region.

3.5. Discussion

Since the internal stress is induced in 95A5B after polarization, fracture toughness of this composite shows anisotropy [10]. Based on this behavior, it is suggested that under the stress level near the fatigue limit (90 MPa) the main toughening mechanism is ferroelastic domain switching, which leads to the development of a process zone near the crack tip. It has been also reported that $BaTiO_3$ has a rising fracture resistance curve [11]. Therefore, it is suggested that the toughening of ferroelectric $BaTiO_3$ is related to the stress-induced domain switching near the crack tip due to the high tensile stress. For a crack parallel to the poling direction, the toughening is related to the stress-induced 90° domain switching process near the crack tip. When a crack propagates, compressive stresses are induced perpendicular to the crack plane because the preferred orientation of the *c*-axis of the tetragonal $BaTiO_3$ is in the direction of tensile stress, as shown in Fig. 10. Compressive stress induced by domain switching normal to the crack surface remains in the crack wake and causes the stress shielding effect at the crack tip. For unpoled 95A5B, the domain orientations of $BaTiO_3$particles are random in Al_2O_3 matrix. Therefore, the compressive stress induced by 90° domain switching is smaller than that in the poled one and then the stress shielding effect is also not so significant compared to the poled one.

At the high stress level, the fatigue life of poled 95A5B became identical to those of unpoled 95A5B and monolithic Al_2O_3. Since the mechanical stressing of piezoelectric materials produces permanent deformation by the irreversible switching of 90° domains, it leads to highly anisotropic deformation behavior for poled materials [12]. Based on the investigation on the behavior of a hard PZT under cyclic mechanical loading [13], the stress-induced domain switching behavior of PZT showed the existence of saturated values of permanent cyclic strain with a strong dependence of the maximum cyclic load. Permanent strains

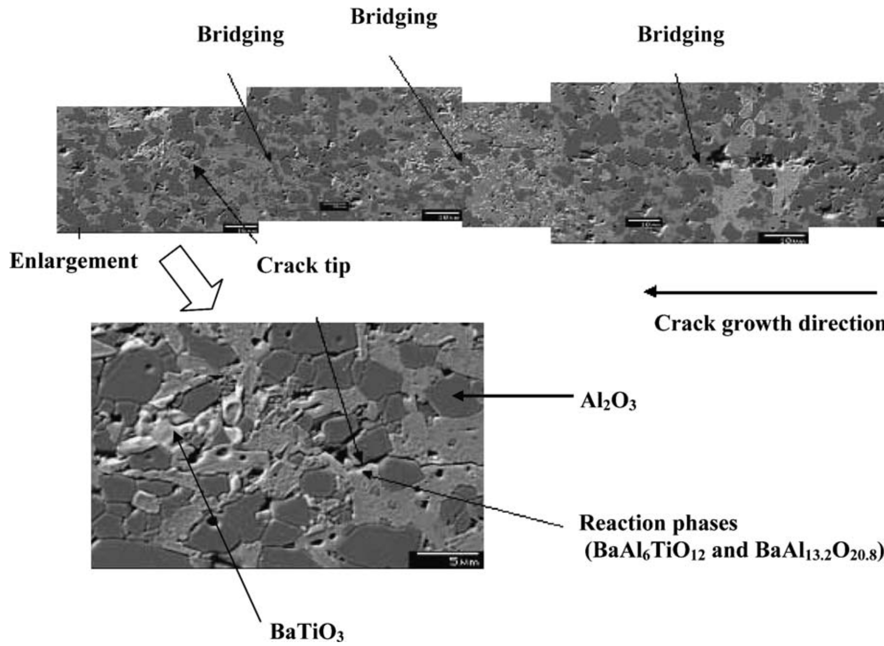

Fig. 9. SEM micrographs of crack path for unpoled 95A5B composite.

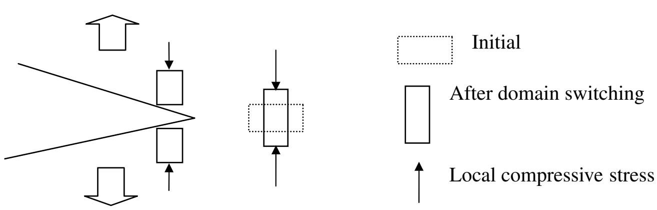

Fig. 10. Schematics of domain switching near a crack tip.

increase very rapidly during cyclic loads over the critical stress for irreversible switching. In the present results, the high mechanical stress would produce permanent strain by irreversible switching of 90° domains. Due to the permanent cyclic strain, which depends on the level of maximum cyclic load, stress-induced domain switching behavior of piezoelectric would saturate and then the stress shielding effect would disappear. Thus, no difference of fatigue strength for these materials was found at high stress levels.

4. Conclusion

Based on the cyclic fatigue test results for the Al_2O_3-based composite with $BaTiO_3$ piezoelectric phase, the following conclusions can be summarized:

1. Fatigue limits of poled and unpoled 95A5B were higher than that of monolithic Al_2O_3, while at higher stress level the fatigue lives of poled, unpoled 95A5B and monolithic Al_2O_3 almost coincided.
2. Fatigue crack growth rate for poled $BaTiO_3$ was lower than that for unpoled sample in the low K_{max} region. At higher K_{max} level, the fatigue crack growth resistance for both unpoled and poled $BaTiO_3$ almost coincided each other. The similar behavior of fatigue crack growth was also observed for unpoled and poled 95A5B. The threshold stress intensity factors for unpoled and poled 95A5B were higher than that of monolithic Al_2O_3 by 9% and 18%, respectively.
3. Fracture surface morphology and crack path profile of the region directly ahead of the crack tip for 95A5B showed a predominantly intergranular crack growth mechanism with grain bridging in the crack wake. The crack was arrested at the reaction phase.
4. The present experimental results strongly suggest that piezoelectric secondary phase significantly improves both fatigue limit and fatigue crack growth resistance, and that the toughening mechanism of $BaTiO_3$–Al_2O_3 composites would be the stress-induced domain switching of piezoelectric secondary phase.
5. At high stress level, the permanent strains are induced by high stress over the critical stress for irreversible domain switching and consequently, the toughening behavior becomes not significant.

Acknowledgments

The authors thank Macoh Co. Ltd. for helping SPS sintering. A part of the present research was supported by the 21st Century COE program of the Ministry of Education, Culture, Sports, Science and Technology of Japan.

References

[1] Nagai T, Hwang HJ, Yasuoka M, Sando M, Niihara K. Preparation of a barium titanate-dispersed-magnesia nanocomposites. J Am Ceram Soc 1998;81(2):425–8.

[2] Chen XM, Yang B. A new approach for toughening of ceramics. Mater Lett 1997;33:237–40.
[3] Yang B, Chen XM. Alumina ceramics toughened by a piezoelectric secondary phase. J Eur Ceram Sci 2000;20:1687–90.
[4] Schneider GA, Heyer V. Influence of the electric field on Vickers indentation crack growth in $BaTiO_3$. J Eur Ceram Soc 1999;19: 1299–1306.
[5] Fang F, Yang W. Poling-enhanced fracture resistance of lead zirconate titanate ferroelectric ceramics. Mater Lett 2000;46: 131–135.
[6] Rattanachan S, Miyashita Y, Mutoh Y. Microstructure and fracture toughness of a spark plasma sintered Al_2O_3-based composite with $BaTiO_3$ particulates. J Eur Ceram Soc 2003;23: 1269–1276.
[7] Mutoh Y. Evaluation and significance of fracture toughness in ceramic materials. ASTM STP 1995;1256:447–60.
[8] Lu W, Fang D-N, Li CQ, Hwang K-C. Nonlinear electric-mechanical behavior and micromechanics modeling of ferroelectric domain evolution. Acta Mater 1999;47(10):2913–26.
[9] Newman Jr JC, Raj JS. An empirical stress-intensity factor equation for the surface crack. Eng Fract Mech 1981;15:185–92.
[10] Rattanachan S, Miyashita Y, Mutoh Y. Effect of polarization fracture toughness of $BaTiO_3/Al_2O^3$ composites. J Eur Ceram Soc 2004;24(5):775–83.
[11] Meschke F, Kolleck A, Scneider GA. R-curve behavior of $BaTiO_3$ due to stress-induced ferroelastic domain switching. J Eur Ceram Soc 1997;17:1143–9.
[12] Calderon-Moreno JM, Guiu F, Meredith M, Reece MJ. Fracture toughness anisotropy of PZT. Mater Sci Eng A 1997;234:1062–6.
[13] Calderon-Moreno JM, Popa M. Stress dependence of reversible and irreversible domain switching in PZT during cyclic loading. Mater Sci Eng 2002;A336:124–8.